Computers and Geotechnics 56 (2014) 160–167

Contents lists available at ScienceDirect

Computers and Geotechnics

journal homepage: www.elsevier.com/locate/compgeo

A simple implementation of RITSS and its application in large deformation analysis

Yinghui Tian *, Mark Jason Cassidy [1], Mark F. Randolph [2], Dong Wang [3], Christophe Gaudin [4]

Centre for Offshore Foundation Systems, The UWA Oceans Institute and ARC CoE for Geotechnical Science and Engineering, University of Western Australia, 35 Stirling Highway, Crawley, Perth, WA 6009, Australia

ARTICLE INFO

Article history:
Received 1 August 2013
Received in revised form 22 October 2013
Accepted 2 December 2013
Available online 22 December 2013

Keywords:
Large deformation
Finite element analysis
Arbitrary Lagrangian Eulerian
RITSS
Python
ABAQUS

ABSTRACT

Large deformation finite element (LDFE) analysis is being applied increasingly in geomechanics as it allows numerical interpretation of problems in which the structural element moves a relatively long distance through the soil. The 'remeshing and interpolation technique with small strain' (RITSS) method for LDFE analysis, in which the soil domain is periodically remeshed with the stress and material properties interpolated from the old to the new within the standard Lagrangian finite element framework, has been successfully applied to a number of practical applications. It allows any standard finite element theory to be used in the Lagrangian analysis, and because the mesh topography and connectivity are not influenced by the previous deforming increment, large deformations are possible. The major barrier of the RITSS method is that the remeshing and interpolation requires specialised and user-dependent computer code. This has limited its application to specialists and hindered its routine application in engineering practice. This paper proposes a simpler, more practical method to implement RITSS for geotechnical applications. By utilising the ABAQUS in-built procedures for interpolation and remeshing, it avoids any need for user-defined code (although a piece of Python script can be used to automate the iteration instead of operating the ABAQUS user interface). A series of four example problems benchmarking this new approach show it to be robust and numerically accurate.

1. Introduction

Numerical modelling of large deformations remains one of the most challenging aspects of geotechnical issues, combining geometric nonlinearity and often material constitutive nonlinearity. This is especially the case for offshore engineering, in which applications such as (but not limited to) full flow penetrometers [37,6,11,56], spudcan penetration [7,42,20], lateral buckling of pipelines [9,49,51], and anchors [35,41,50,4,53] involve significant relative displacement of the structural element through the soil.

Various approaches for large deformation finite element (LDFE) analysis have been proposed over the last three decades. Early developments from the small strain to finite strain measurements comprised the total Lagrangian [18] and updated Lagrangian [1,31,23] approaches, both of which were limited by excessive distortion of elements as the analysis progressed due to the Lagrangian formulation. A radically different formulation is the Eulerian method, which allows material to flow through a fixed spatial mesh. The rare examples of the Eulerian method that can be found in the literature on solid mechanics are the early developments [32,14,13,47] and some recent applications with the commercial software ABAQUS [43,36,46]. The challenging obstacles of the Eulerian formulation lie in its poor ability to deal with free surfaces, material interfaces and heterogeneous materials (e.g., offshore sediments exhibiting an increasing shear strength with depth). Combining the merits of both the Lagrangian and Eulerian approaches, the arbitrary Lagrangian Eulerian (ALE) approach has been applied to solid mechanics by, among others, Liu et al. [26,27], Ghosh [15,16], and Ghosh and Kikuchi [17] and by Nazem et al. [34] in geomechanics. These ALE developments have tended to follow a formal approach, with finite strain formulations for the Lagrangian steps and incorporating "convection" of the soil relative to the finite element mesh implicitly in the finite element equations [39]. Recently, Kardani et al. [24,25] incorporated h-adaptive meshing technique into their in-house developed ALE programs to improve the numerical accuracy.

The 'remeshing and interpolation technique with small strain' (RITSS) approach proposed by Hu and Randolph [22] falls within

* Corresponding author. Tel.: +61 8 6488 7076; fax: +61 8 6488 1044.
E-mail addresses: yinghui.tian@uwa.edu.au (Y. Tian), mark.cassidy@uwa.edu.au (M.J. Cassidy), mark.randolph@uwa.edu.au (M.F. Randolph), dong.wang@uwa.edu.au (D. Wang), christophe.gaudin@uwa.edu.au (C. Gaudin).
[1] Tel.: +61 8 6488 3732; fax: +61 8 6488 1044.
[2] Tel.: +61 8 6488 3075; fax: +61 8 6488 1044.
[3] Tel.: +61 8 6488 3447; fax: +61 8 6488 1044.
[4] Tel.: +61 8 6488 7289; fax: +61 8 6488 1044.

0266-352X/$ - see front matter © 2013 Elsevier Ltd. All rights reserved.
http://dx.doi.org/10.1016/j.compgeo.2013.12.001

the ALE category. However, it has distinct advantages as it is based on standard Lagrangian increments with periodic remeshing, followed by interpolation of all stresses and material properties. Thus, the new mesh topology and connectivity is not influenced by the previous increment. The independence of the remeshing and interpolation from the preceding Lagrangian incremental analysis allows any standard finite element program to be used. These distinct features render RITSS relatively robust and versatile in practical applications (such as, among others, [21,48,19,57,56,49,51,52]).

The implementation of RITSS generally involves four steps [39]: (1) initial mesh generation, (2) incremental step of Lagrangian analysis, (3) updating boundaries and remeshing, and (4) mapping of stresses and material properties from the old to new mesh. In any analysis, steps (2)–(4) are repeated until completion of the whole LDFE analysis. As a standard Lagrangian analysis process, step (2) can be conducted with any Lagrangian finite element package. Early realisations were built around the finite element program AFENA [3] to fulfil the functionality of step (2). More recently, commercial finite element packages have been employed, including ABAQUS [49,51] and LS-DYNA [28]. Steps (1) and (3) are essentially pre-processing and preparing the finite element model, which usually can be performed with the affiliated pre-processor of the Lagrangian finite element package or via third party software (e.g., ANSYS was adopted in [54]). The interpolation and mapping procedure of step (4) is pivotal, as it is largely related to the accuracy of the whole RITSS analysis. Currently available RITSS implementations require users to write in-house code for mapping field variables from the old to new mesh, which has been the largest barrier to wider application of the RITSS approach. This is especially challenging for the inexperienced user, as inappropriate or less rigorously coded subroutines in step (4) can lead to unacceptable errors or even numerical instabilities when running the program.

This paper proposes a practical implementation of RITSS using the commercial package ABAQUS that avoids user coding for mapping of stresses and material properties from the old to new mesh (the aforementioned step (4)). This simple implementation approach involves the adoption of an ABAQUS built-in technique, namely 'mesh-to-mesh solution mapping' (abbreviated as MSM in this paper). The following sections detail firstly the implementation, followed by four analysis examples to benchmark and validate the approach against available published results. Because the current RITSS implementations require user coding for step (4), the overall goal of this paper is to demonstrate the present simplified RITSS implementation and facilitate readers to conduct their own LDFE analysis.

2. Implementation framework

The built-in technique in ABAQUS, MSM, is able to map field variables from the old to new mesh. The field variables include the stresses, material properties at the integration points, and temperature at element nodes. According to Dassault Systèmes [8], initially, MSM involves associating solution variables with nodes in the old mesh. For nodal solution variables (e.g., nodal temperature or pore pressure), the association is already made. For integration point variables (e.g., stress), the solution variables at the nodes of the old mesh are obtained by extrapolating values from the integration points to the nodes of each element and then averaging these values over all similar elements abutting each node. Following this, the location of each node and integration point in the new mesh is obtained with respect to the old mesh. The variables (including stresses and material properties) are then interpolated from the nodes of the old element to the integration points or nodes in the new mesh.

The four steps of RITSS implementation summarised by Randolph et al. [39] are realised in the following manner here: (i) an initial finite element model in terms of original soil geometry is built with geostatic equilibrium being established (if applicable) and the first incremental displacements and forces are applied; (ii) the displaced position of structural elements and soil boundaries and interfaces are extracted from the ABAQUS result file; (iii) a new finite element model is created based on the deformed geometry and remeshed; (iv) the stresses and material properties are mapped to the new mesh by writing the keyword of MSM into the ABAQUS input file; and (v) the input file is run for another incremental step of displacement or force. Steps (ii)–(v) are repeated until the analysis is finished. With the built-in MSM, i.e., step (iv) in this procedure, to fulfil the mapping solution without user coding, the whole LDFE simulation can be conducted with ABAQUS/CAE (the user interface for pre-processing, submitting the analysis, and post-processing). However, writing one piece of ABAQUS Python script (see Dassault Systèmes [8] for details about this extended Python language) the multiple iterations required in the LDFE can be automated (rather than operating manually in ABAQUS/CAE). This script can be submitted to ABAQUS for running without user intervention. An example of such a Python script is provided in Table 1, with further explanation provided under example 1.

3. Analysis examples

Four analysis examples are presented to provide benchmarking with available publications to show the accuracy of this proposed approach. These represent a wide range of geometries and include (i) deep penetration of a T-bar penetrometer; (ii) penetration of a surface footing; (iii) keying of a plate anchor; and (iv) penetration of pipelines considering soil heterogeneity, rate effect, and strain softening. The intention of presenting these examples in this paper is not to provide additional insight into the problems themselves, but to demonstrate the proposed RITSS implementation and to verify its accuracy against known solutions. Table 1 shows the skeleton of the ABAQUS scripting code for example 1 (T-bar deep penetration). This can be used as a reference for readers to solve their own problems.

In all benchmark cases, the soil is modelled as a Tresca material with an undrained shear strength of s_u (homogenous or increasing with depth) and Young's modulus of $E = 500s_u$ (unless otherwise stated). A Poisson ratio of $\nu = 0.49$ is taken to approximate undrained conditions. The soil is meshed as 8-node quadrilateral elements with reduced integration for two dimensional plane strain modelling and 8-node linear bricks with reduced integration for three dimensional modelling. The structural elements are simplified as a rigid body. Three dimensional 8-node linear brick reduced integration element has only one single integration point. During the extrapolation process, the value at the single integration point is used directly for each node of that element. Averaging over the abutting elements, nevertheless, can cause the solution variables to vary from node to node. The material properties (such as the undrained shear strength s_u, if not homogeneous) are defined as field variables at each node, with the material (and its properties) moving with the mesh. Following remeshing, the material properties are mapped from the old element node to the new element node using interpolation.

3.1. Deep penetration of a T-bar penetrometer

As a full-flow penetrometer, the T-bar is being used increasingly in geotechnical investigations, as it provides a robust factor for interpreting the soil strength from the penetration resistance. This

Table 1
Script skeleton Example 1 (T-bar penetration).

(i) Initial model with an increment of penetration

```
from abaqus import *
from abaqusConstants import *
import os
mymodel=mdb.models['Model-1']
soilpart=mymodel.Part(dimensionality=TWO_D_PLANAR, name='SoilPart', type=DEFORMABLE_BODY)
Tbarpart=mymodel.Part(dimensionality=TWO_D_PLANAR, name='TbarPart', type=DEFORMABLE_BODY)
mymodel.Material(name='SoilMat')
mymodel.Material(name='TbarMat')
mymodel.rootAssembly.Instance(dependent=ON, name='TbarPart-1', part=Tbarpart)
mymodel.rootAssembly.Instance(dependent=ON, name='SoilPart-1', part=soilpart)
mymodel.GeostaticStep(name='Geo', previous='Initial')
mymodel.StaticStep(initialInc=0.001, name='Penetration', previous='Geo',maxInc=0.1, maxNumInc=10,000)
mdb.models['Model-1'].parts['SoilPart'].setElementType(elemTypes=(ElemType(elemCode=CPE8R, elemLibrary=STANDARD),
ElemType(elemCode=CPE6M, elemLibrary=STANDARD)), regions=(mdb.models['Model-1'].parts['SoilPart'].faces,))
mdb.models['Model-1'].parts['SoilPart'].seedEdgeByBias(endlEdges=myEdges, minSize=0.009, maxSize=0.04)
mdb.models['Model-1'].parts['SoilPart'].generateMesh()
...
myjob=mdb.Job(model='Model-1', name='Mesh0',OutputPrecision=FULL)
myjob.submit()
...
```

(ii) Extracting deformed geometry and boundary conditions

```
for i in range(NMesh):
  #read the Tbar displacement and track the free boundary
  lstOdbname= Mesh'+str(i)+'.odb'
  lstOdb=session.openOdb(name=lstOdbname)
  dx[0]=lstOdb.steps['Penetration'].frames[-1].fieldOutputs['U'].getSubset(region=myset).values[0].dataDouble[0]
  dy[0]=lstOdb.steps['Penetration'].frames[-1].fieldOutputs['U'].getSubset(region=myset).values[0].dataDouble[1]
  ...
```

(iii) Remeshing and setting up new model

```
#create new model
mymodel=mdb.models['Model-1']
mymodel.parts['TbarPart'].generateMesh()
mymodel.parts['SoilPart'].generateMesh()
mymodel.GeostaticStep(name='Geo', previous='Initial')
mymodel.StaticStep(initialInc=0.001, name='Penetration', previous='Geo',maxInc=0.1, maxNumInc=10,000)
...
```

(iv) Mesh-to-mesh solution mapping

```
mdb.Job(model='Model-1', name='Scratch'+str(i+1), nodalOutputPrecision=FULL)
mdb.jobs['Scratch'+str(i+1)].writeInput()
infile=open('Scratch'+str(i+1)+'.inp','r')
outfile=open('Mesh'+str(i+1)+'.inp','w')
...
outfile.write('*Map solution/n')
infile.close()
outfile.close()
...
```

(v) Conducting small increment of penetration

```
os.system('abaqus job=Mesh'+str(i+1)+' oldjob=Mesh'+str(i)+ ' output_precision=full int')
```

example simulated the deep penetration process of a T-bar, such as published in Tian et al. [46] using in-house coded RITSS (see [51] for details about the implementation, which requires user coding of the solution mapping process). The T-bar had a diameter $D = 0.04$ m (as typically used in the offshore industry [29]) and was 'wished in place' with an initial embedment of $4.5D$, sufficient to lead to a 'full-flow' mechanism during penetration. The undrained shear strength of the soil was uniform with $s_u = 5$ kPa. The interface between the T-bar and the soil was modelled as frictionless and fully bonded, respectively. As shown in Fig. 1, only half of the T-bar and soil domain was modelled to take advantage of the symmetry. The width and height of the soil domain was taken as $10D$, and the soil bottom was fixed, whereas the lateral soil was 'roller supported', allowing vertical movement. The minimum element size h_{min} was set as $D/20$, which is the same as in Tian et al. [46] allowing direct comparison.

The calculated relationship between the normalised soil resistance V/Ds_u and the normalised embedment w/D is shown in Fig. 2. The ultimate bearing capacity factor V_{ult}/Ds_u was calculated as 9.22 and 12.31 for frictionless contact and fully bonded conditions respectively. According to Randolph and Houlsby [38], Einav and Randolph [11], and Martin and Randolph [30], the upper and lower bound solutions are 9.14 and 9.20 for the frictionless contact condition. For the fully bonded condition, the upper and lower bounds coincide as 11.94 (and thus provide an exact solution). Also shown in Fig. 2 are the published LDFE results of Tian et al. [46]. Considering the nature of the displacement finite element method, LDFE is expected to be close to the upper bound solution. From the comparison, this study does indeed show closer agreement with the upper bound solution (exact solution for the fully bonded case). To further demonstrate the performance of the method proposed, finer meshing was used with minimum element size $h_{min} = D/50$. The calculated ultimate bearing capacity factors were improved to 9.21 and 12.04 for the frictionless and fully bonded cases respectively (see Table 2 for details). This verifies that the proposed simple implementation of RITSS is capable of achieving good accuracy. In this example, the whole analysis consists of 40 remeshing steps and the number of soil elements was kept around 6600 in each step. The analysis took 50 minutes to complete on a desktop computer (2.8 Hz CPU and 8 GB memory) with a single CPU thread.

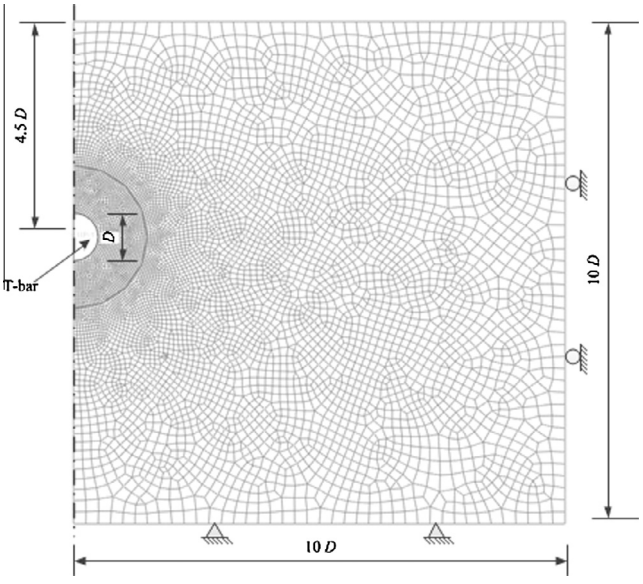

Fig. 1. T-bar finite element model and meshing.

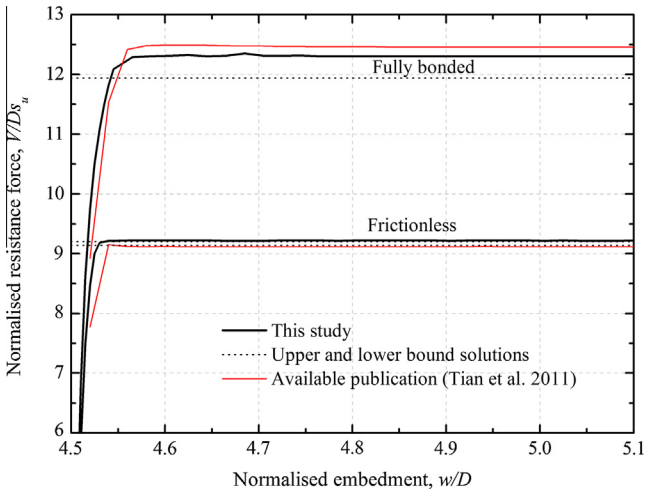

Fig. 2. T-bar resistance capacity.

3.2. Penetration of surface footing

This example simulated the penetration of a surface footing into weightless homogeneous soil. It is compared to results published by Nazem et al. [33], which used an in-house developed ALE program. The undrained shear strength of soil was $s_u = 1$ kPa with Young's modulus of $E = 100s_u$. To take advantage of the symmetry, only half of the footing and soil domain was used (see Fig. 3). The soil domain was taken as $12 \times 8B$, with the soil bottom fixed and the lateral soil 'roller supported'. A finer mesh was used close to the footing, with a minimum element size h_{min} of $B/8$. Again, the mesh was set to be the same as used in Nazem et al. [33].

The calculated normalised vertical resistance V/Bs_u against penetration w/B is plotted in Fig. 4 and compared with the result of the static analysis in Nazem et al. [33]. In general, the results agree quite well with those from Nazem et al. [33] when the penetration is less than $0.17B$. After that, the resistance force from this study becomes lower than from Nazem et al. [33] but still increases slowly. The analysis of Nazem et al. [33] terminated when the penetration reached approximately $0.225B$ at which stage the normalised resistance V/Bs_u was approximately 6.25. Nazem et al. [33] described this lack of convergence in the ALE method as an indication of reaching the ultimate load. In contrast, no convergence problem was met in the present analysis, with the penetration continuing to the specified value of $0.3B$.

3.3. Keying of a plate anchor

Plate anchors used offshore are often installed in a vertical orientation and then are gradually 'keyed' (i.e., rotated) under the action of the mooring line, which is attached to a padeye offset from the plane of the anchor. Fig. 5 illustrates a suction embedded plate anchor [10], in which a suction caisson is used to install the plate anchor. This example simulated the anchor keying process of the centrifuge test in Song et al. [40], comparing it with the available LDFE analysis in Wang et al. [50] (again, the Wang et al. [50] analysis used in-house coding of the mapping solution in the LDFE analysis).

In the centrifuge test, a square anchor was used simulating the height (and also width) B of 4 m and thickness t of 0.2 m of a typical prototype anchor. The padeye eccentricity e (measuring from the padeye to the anchor front face) was 2.5 m and the unit weight of the anchor material was 77 kN/m^3. Transparent soil was used with a uniform undrained shear strength of $s_u = 18$ kPa and a unit weight of 9.23 kN/m^3. The anchor was pulled vertically from the

Table 2
Comparison of T-bar penetration resistance factors.

Contact condition	Lower bound	Upper bound	Tian et al. [46] $h_{min} = D/20$	This study	
				$h_{min} = D/20$	$h_{min} = D/50$
Frictionless	9.14	9.2	9.15	9.22	9.21
Fully bonded	11.94		12.46	12.31	12.04

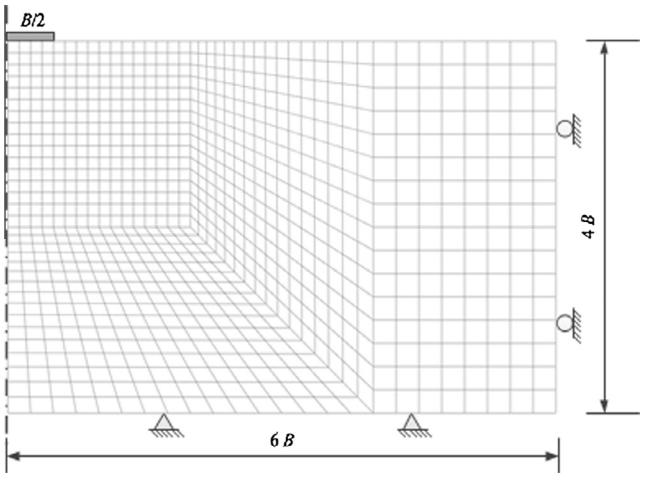

Fig. 3. Surface footing initial finite element model.

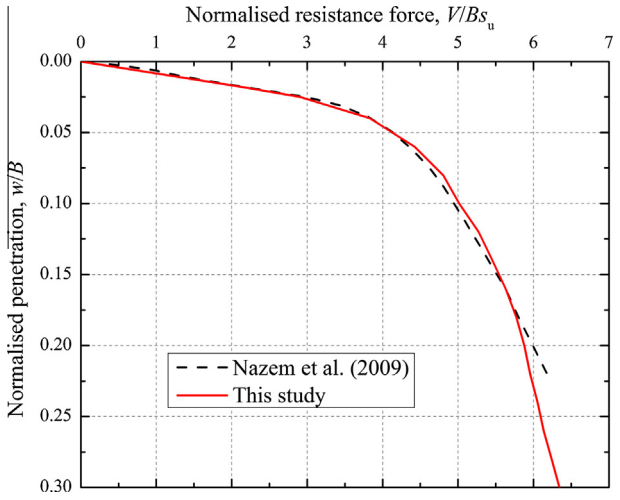

Fig. 4. Surface footing resistance versus penetration.

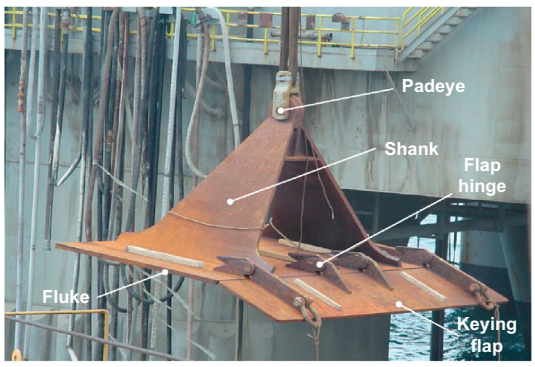

Fig. 5. Suction embedded plate anchor.

padeye. In this study, both strip (two dimensional plane strain condition) and square anchor (three dimensional condition) were accounted. The shank was omitted to be consistent with Wang et al. [50], which is also a common practice in the current literature of plate anchors (see [2,44,45,35,12,41], and discussion in [4]). The interface between the anchor and the soil was modelled as fully bonded. The minimum element length h_{min} in the model was $t/2$ (strip anchor) and t (square anchor). The calculation soil domain is as shown in Fig. 6, which is considered as large enough to eliminate boundary effects. For the plane strain strip anchor, the top soil surface was tracked and updated with the LDFE analysis process. In the three dimensional modelling (Fig. 6b), the top soil surface was not updated but kept at the original position. This approximation saved numerical effort to track the nodes and elements on the top of the soil surface. It is an acceptable approxima-

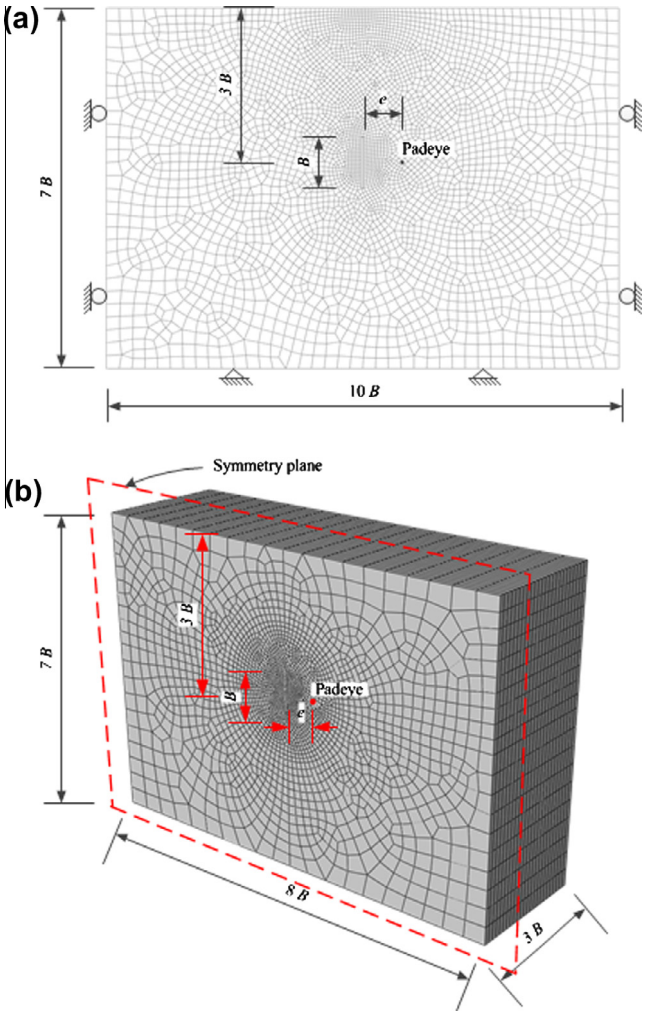

Fig. 6. Anchor model and meshing. (a) Two dimensional plane strain model. (b) Three dimensional model.

tion when the anchor is deeply buried. In this study, half anchor with $B/2$ width was used to take advantage of the symmetry.

The calculated results of the relationship between the normalised anchor displacement Δz_c (measuring at the anchor centre) and the anchor inclination angle β are shown in Fig. 7, with the inset illustrating the symbol convention. The available LDFE results of Wang et al. [50] and the centrifuge test of Song et al. [40] are also shown in the figure for comparison. In general, good agreement between this study and Wang et al. [50] can be observed for both strip and square anchor cases. Due to the symmetry of the anchor and homogeneity of the soil, the anchor is expected to become horizontal (perpendicular to the vertical pulling direction) when the keying process finishes. However, the final anchor inclination in the centrifuge test was approximately 11°, which was thought to be due to the fixed pulley, and thus not strictly vertical chain after keying [50]. This study shows a smoother 'levelling-out' of the curve when the keying finishes for both the two dimensional strip and the three dimensional square anchor.

The calculated normalised resistance pulling force F/As_u is plotted against the chain displacement in Fig. 8, where the anchor area A is taken as B for the strip anchor case. Also shown are the LDFE results of Wang et al. [50] and the centrifuge test of Song et al. [40]. Very good agreement can be seen between this study and Wang et al. [50] for the strip anchor. For the square anchor, the present study predicts a smaller pulling load during the early stages of keying but agrees well with Wang et al. [50] as the keying progresses. The calculated anchor capacity factor F/As_u was calculated as 12.60 and 15.01 in this study for strip and square anchor cases, respectively. If the effect of the submerged weight of steel in soil $(77-9.23)\times 0.2/18 = 0.75$ is subtracted, these values are 11.85 and 14.26, respectively. These agree well with the values of 11.87 ([35] for strip anchor) and 14.15 [49]. The centrifuge test of Song et al. [40] gave lower resistance than from the numerical solutions, which was considered to be because of the shear strength reduction due to anchor installation disturbance and keying [50]. In the three dimensional analysis, a total 60 iterations of remeshing were conducted and approximately 50,000 soil elements were used in each step. The whole analysis running time was about 20 h on a desktop computer with a single CPU thread.

3.4. Penetration of shallowly embedded pipelines

Accurate assessment of the penetration of offshore pipelines is essential for assessing their on-bottom stability, lateral buckling,

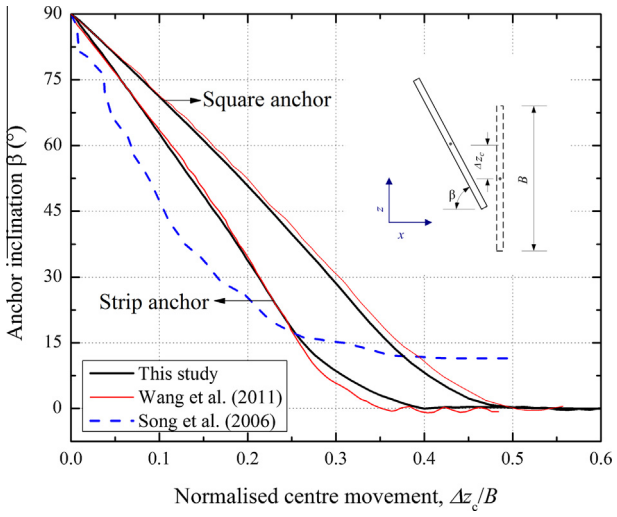

Fig. 7. Anchor movement versus anchor inclination (modelling [41].

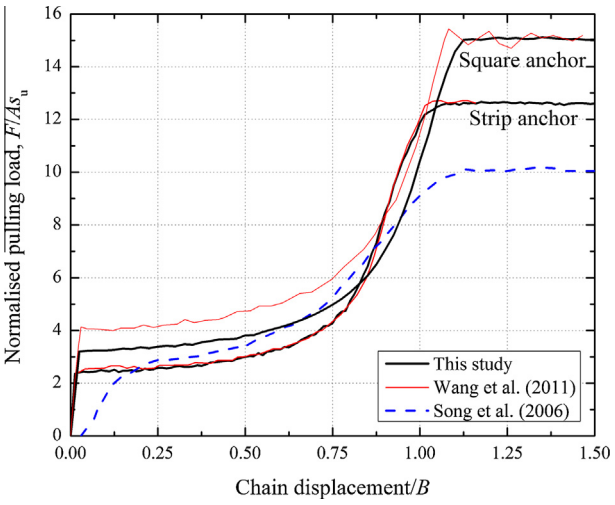

Fig. 8. Normalised uplift resistance.

and axial walking behaviour. Dingle et al. [9] carried out centrifuge tests including particle image velocimetry and photogrammetry to investigate the pipeline mechanism. The pipe had a diameter $D = 0.8$ m at prototype scale, and it was penetrated a half diameter from the soil surface. The soil was characterised using a T-bar penetrometer, which showed the shear strength s_{u0} increased linearly with depth according to $s_{u0} = s_{um} + kz$, where $s_{um} = 2.3$ kPa is the intact undrained shear strength at the soil surface, and $k = 3.6$ kPa/m is the soil strength gradient. The soil had a unit weight of 6.5 kN/m^3. Chatterjee et al. [5] reported an LDFE analysis with in-house developed RITSS coding to retrospectively simulate the centrifuge test. The soil heterogeneity (increasing shear strength with depth), strain rate effect, and strain softening effect were accounted for in their analysis. This example is presented to show the performance of the proposed simple RITSS method for complex soil conditions by comparing with Chatterjee et al. [5] and the centrifuge test results.

In this example, a half model was used to take advantage of the symmetry, and the calculated domain was taken as $6.5\times 5D$. The maximum shear strength between the pipe and soil interface was considered to be $0.31s_{um}$, as adopted by Chatterjee et al. [5]. The minimum element size $h_{\min}$ was taken as $D/16$ so that the model setup agrees closely with Chatterjee et al. [5]. Fig. 9 shows the initial mesh of the finite element model. Fig. 10 shows the calculated relationship between the normalised resistance force V/Ds_{u0} and the penetration depth w/D compared with the LDFE results of Chatterjee et al. [5]. Very good agreement can be seen for the no strain rate or softening case.

To further benchmark the approach proposed, the effect of strain rate and strain softening was taken into account according to [11,55]:

$$s_u = \left[1+\mu\log\left(\frac{\max(\dot{\gamma}_{\max},\dot{\gamma}_{ref})}{\dot{\gamma}_{ref}}\right)\right]\left[\delta_{rem}+(1-\delta_{rem})e^{-3\xi/\xi_{95}}\right]s_{u0} \quad (1)$$

where the rate parameter $\mu = 0.1$, $\dot{\gamma}_{ref} = 3\times 10^{-6}\,\mathrm{s}^{-1}$; $\delta_{rem} = 1/S_t$, (the sensitivity $S_t = 3.2$); ξ is the accumulated absolute plastic shear strain and $\xi_{95} = 10$. The maximum shear strain rate $\dot{\gamma}_{\max}$ is defined as:

$$\dot{\gamma}_{\max} = \frac{(\Delta\varepsilon_1-\Delta\varepsilon_3)}{\delta/D}\frac{v_p}{D} \quad (2)$$

where $\Delta\varepsilon_1$ and $\Delta\varepsilon_3$ are major and minor principal strains resulting from a displacement increment δ and v_p is the pipe velocity.

The calculation results including strain rate and softening effects are also plotted in Fig. 10 and compared with Chatterjee

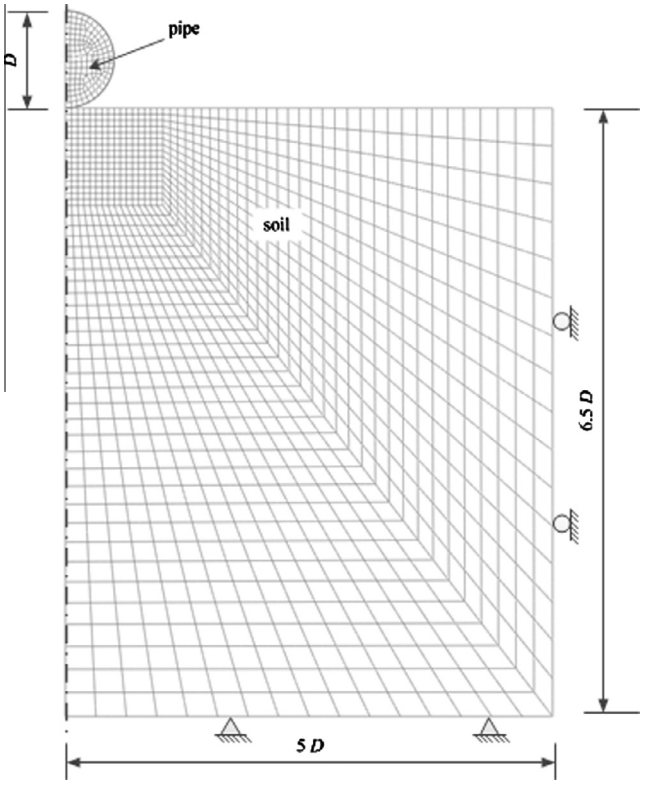

Fig. 9. Pipeline finite element model and meshing.

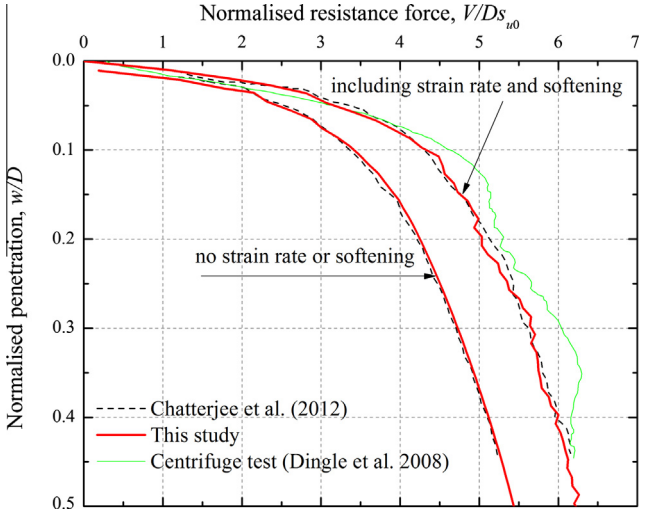

Fig. 10. Pipe resistance versus penetration.

et al. [5] and the centrifuge test of Dingle et al. [9]. The present analysis shows a slightly less smooth curve than evaluated by Chatterjee et al. However, excellent agreement with Chatterjee et al. [5] was achieved in general.

4. Concluding remarks

This paper has presented an alternative development of the RITSS approach for large deformation finite element analysis and demonstrates the performance with four examples. The good agreement with published results from existing publications and centrifuge model tests has validated the accuracy of this proposed approach. As a built-in technique within ABAQUS, the running of MSM is extremely fast and the whole analysis time is acceptable for desktop computers as demonstrated in the calculation examples. Obviously, the total running time of a LDFE analysis depends mainly on computational cost of each Lagrangian calculation (which in turn depends on the number of elements and degrees of freedom). No numerical or convergence problems were met during the analysis, which shows its efficiency and robustness of the proposed LDFE approach. It is considered to be worthwhile to point out that one important issue in large deformation finite element analysis is to accurately and efficiently track the deformed soil geometry such as the soil free surface. Essentially, it is a problem of how to track the positions of key element nodes, which is involved in the Python coding.

This proposed simple approach for implementing RITSS avoids the effort of coding specialist meshing and mapping solution subroutines. Taking advantage of the functionality available in the commercial package ABAQUS, complex LDFE analysis can be conducted with a short segment of Python script to automate the iteration. Sufficient details of the method, together with skeleton Python code, have been presented to allow users to apply the method to their own large deformation problems in geotechnics.

Acknowledgements

This research was undertaken with support from the Australia-China Natural Gas Technology Partnership Fund and the Lloyd's Register Foundation (LRF). LRF a UK registered charity and sole shareholder of Lloyd's Register Group Ltd, invests in science, engineering and technology for public benefit, worldwide. The work also forms part of the activities of the Australian Research Council Centre of Excellence for Geotechnical Science and Engineering. The help from Dr. S. Chatterjee at COFS and discussion about ABAQUS technical issues from Mr. J. Su in Wuxi and Professor C. Zhang in HBUST of China (during the corresponding author's academic visiting supported by NSFC project 51274079), are much appreciated.

References

[1] Bathe KJ, Ramm E, Wilson EL. Finite element formulations for large deformation dynamic analysis. Int J Numer Methods Eng 1975;9:353–86.
[2] Bransby MF, O'Neill M. Drag anchor fluke soil interaction in clays. In: Proc 7th int symp on numerical models in geomechanics, Graz, 1999. p. 489–94.
[3] Carter JP, Balaam NP. Afena user manual 5.0. Geotechnical Research Centre, The University of Sydney; 1995.
[4] Cassidy MJ, Gaudin C, Randolph MF, Wong PC, Wang D, Tian Y. A plasticity model to assess the keying behaviour and performance of plate anchors. Geotechnique 2012;62(9):825–36.
[5] Chatterjee S, Randolph MF, White DJ. The effects of penetration rate and strain softening on the vertical penetration resistance of seabed pipelines. Geotechnique 2012;62(7):573–82.
[6] Chung SF, Randolph MF, Schneider JA. Effect of penetration rate on penetrometer resistance in clay. J Geotech GeoEnviron Eng ASCE 2006;132(9):1188–96.
[7] Craig WH, Chua K. Deep penetration of spud-can foundations on sand and clay. Geotechnique 1990;40(4):541–56.
[8] Dassault Systèmes. Abaqus analysis user's manual. RI: SIMULIA, Providence; 2010.
[9] Dingle HRC, White DJ, Gaudin C. Mechanisms of pipe embedment and lateral breakout on soft clay. Can Geotech J 2008;45(5):636–52.
[10] Dove P, Treu H, Wilde B. Suction embedded plate anchor (SEPLA): a new anchoring solution for ultra-deepwater mooring. In: Proc deep offshore technology conference, New Orleans, 1998.
[11] Einav I, Randolph MF. Combining upper bound and strain path methods for evaluating penetration resistance. Int J Numer Meth Eng 2005;63(14):1991–2016.
[12] Elkhatib S, Randolph MF. The effect of interface friction on the performance of drag-in plate anchors. In: Proc 5th int symp on frontiers in offshore geotechnics, Perth, 2005. p. 171–7.
[13] Gadala MS, Dokainish MA, Oravas GA. Formulation methods of geometric and material nonlinearity problems. Int J Numer Meth Eng 1984;20(5):887–914.
[14] Gadala MS, Oravas GA, Dokainish MA. A consistent Eulerian formulation of large deformation problems in static and dynamics. Int J Non-lin Mech 1983;18:21–35.

[15] Ghosh S. Finite element simulation of some extrusion processes using the arbitrary Lagrangian–Eulerian description. J Mater Shaping Technol 1990;8:53–64.
[16] Ghosh S. Arbitrary Lagrangian–Eulerian finite-element analysis of large deformation in contacting bodies. Int J Numer Meth Eng 1992;33(9):1891–925.
[17] Ghosh S, Kikuchi N. An arbitrary Lagrangian–Eulerian finite-element method for large deformation analysis of elastic-viscoplastic solids. Comput Methods Appl Mech Eng 1991;86(2):127–88.
[18] Hibbitt HD, Marcal PV, Rice JR. A finite element formulation for problems of large strain and large displacement. Int J Solid Struct 1970;6:1069–86.
[19] Hossain MS, Hu Y, Randolph MF, White DJ. Limiting cavity depth for spudcan foundations penetrating clay. Geotechnique 2005;55(9):679–90.
[20] Hossain MS, Randolph MF. New mechanism-based design approach for spudcan foundations on single layer clay. J Geotech Geoenviron Eng 2009;135(9):1264–74.
[21] Hu Y, Randolph MF. Deep penetration of shallow foundations on nonhomogeneous soil. Soils Found 1998;38(1):241–6.
[22] Hu Y, Randolph MF. A practical numerical approach for large deformation problems in soil. Int J Numer Anal Meth Geomech 1998;22(5):327–50.
[23] Hughes TJR, Winget J. Finite rotation effects in numerical-integration of rate constitutive-equations arising in large-deformation analysis. Int J Numer Meth Eng 1980;15(12):1862–7.
[24] Kardani M, Nazem M, Abbo AJ, Sheng D, Sloan SW. Refined h-adaptive finite element procedure for large deformation geotechnical problems. Comput Mech 2012;49(1):21–33.
[25] Kardani M, Nazem M, Sheng D, Carter JP. Large deformation analysis of geomechanics problems by a combined rh-adaptive finite element method. Comput Geotech 2013;49:90–9.
[26] Liu WK, Belytschko T, Chang H. An arbitrary Lagrangian–Eulerian finite-element method for path-dependent materials. Comput Methods Appl Mech Eng 1986;58(2):227–45.
[27] Liu WK, Chang H, Chen JS, Belytschko T. Arbitrary Lagrangian–Eulerian Petrov-Galerkin finite-elements for nonlinear continua. Comput Methods Appl Mech Eng 1988;68(3):259–310.
[28] Liyanapathirana DS. Numerical simulation of T-Bar penetration in soft clay. In: Proc GeoCongress 2008, New Orleans, 2008.
[29] Low HE, Lunne T, Andersen KH, Sjursen MA, Li X, Randolph MF. Estimation of intact and remoulded undrained shear strength from penetration tests in soft clays. Géotechnique 2010;60(11):843–59.
[30] Martin CM, Randolph MF. Upper-bound analysis of lateral pile capacity in cohesive soil. Geotechnique 2006;56(2):141–5.
[31] McMeeking RM, Rice JR. Finite element formulations for problems of large elastic–plastic deformation. Int J Solids Struct 1975;11:601–16.
[32] Nagtegaal JC, Dejong JE. Some computational aspects of elastic–plastic large strain analysis. Int J Numer Meth Eng 1981;17(1):15–41.
[33] Nazem M, Carter JP, Airey DW. Arbitrary Lagrangian–Eulerian method for dynamic analysis of geotechnical problems. Comput Geotech 2009;36(4):549–57.
[34] Nazem M, Sheng DC, Carter JP. Stress integration and mesh refinement for large deformation in geomechanics. Int J Numer Meth Eng 2006;65(7):1002–27.
[35] O'Neill MP, Bransby MF, Randolph MF. Drag anchor fluke–soil interaction in clays. Can Geotech J 2003;40(1):78–94.
[36] Qiu G, Henke S, Grabe J. 3D FE analysis of the installation process of spudcan foundations. Frontiers in offshore geotechnics II, Perth, Australia, Taylor & Francis Group.
[37] Randolph MF. Characterisation of soft sediments for offshore applications. In: Keynote paper, proc. 2nd int conf on site characterisation, Porto, Portugal, 2004.
[38] Randolph MF, Houlsby GT. The limiting pressure on a circular pile loaded laterally in cohesive soil. Geotechnique 1984;34(4):613–23.
[39] Randolph MF, Wang D, Zhou H, Hossain MS, Hu Y. Large deformation finite element analysis for offshore applications. In: Proc 12th int conf of the int association for computer methods and advances in geomechanics, IACMAG, Goa, India, 2008.
[40] Song Z, Hu Y, Wang D, O'Loughlin CD. Pullout capacity and rotational behaviour of square anchors. In: Proc 6th int conf physical modelling in geotechnics, Hong Kong, 2006. p. 1325–31.
[41] Song Z, Hu Y, O'Loughlin C, Randolph MF. Loss in anchor embedment during plate anchor keying in clay. J Geotech Geoenviron Eng 2009;135(10):1475–85.
[42] Teh KL, Cassidy MJ, Leung CF, Chow YK, Randolph MF, Quah CK. Revealing the bearing capacity mechanisms of a penetrating spudcan through sand overlying clay. Geotechnique 2008;58(10):793–804.
[43] Tho KK, Leung CF, Chow YK, Swaddiwudhipong S. Application of Eulerian finite element technique for analysis of spudcan and pipeline penetration into the seabed. The Jack-up platform design, construction and operation, London, 2009.
[44] Tian Y, Gaudin C, Cassidy MJ, Randolph MF. Considerations on the Design of Keying Flap of Plate Anchors. J Geotech Geoenviron Eng ASCE 2013;139(7):1156–64.
[45] Tian Y, Gaudin C, Cassidy, MJ. Improving Plate Anchor Design with a Keying Flap. J Geotech Geoenviron Eng ASCE, 2013, submitted for publication.
[46] Tian Y, Wang D, Cassidy MJ. Large deformation finite element analysis of offshore penetration tests. In: The second international symposium on computational geomechanics (ComGeo II), Cavtat-Dubrovnik, Croatia, 2011.
[47] van den Berg P, de Borst R, Huetink H. An Eulerian finite element model for penetration in layered soil. Int J Numer Analyt Meth Geomech 1996;20:865–86.
[48] Wang CX, Carter JP. Deep penetration of strip and circular footings into layered clays. Int J Geomech ASCE 2002;2(2):205–32.
[49] Wang D, Hu YX, Randolph MF. Three-dimensional large deformation finite-element analysis of plate anchors in uniform clay. J Geotech Geoenviron Eng 2010;136(2):355–65.
[50] Wang D, Hu Y, Randolph MF. Keying of rectangular plate anchors in normally consolidated clays. J Geotech Geoenviron Eng 2011;137(12):1244–53.
[51] Wang D, White DJ, Randolph MF. Large-deformation finite element analysis of pipe penetration and large-amplitude lateral displacement. Can Geotech J 2010;47(8):842–56.
[52] Wang D, Randolph MF, White DJ. A dynamic large deformation finite element method based on mesh regeneration. Comput Geotech 2013;54:192–201.
[53] Yang M, Aubeny CP, Murff JD. Behavior of suction embedded plate anchors during keying process. J Geotech Geoenviron Eng 2012;138(2):174–83.
[54] Yu L, Liu J, Kong XJ, Hu Y. Three-dimensional RITSS large displacement finite element method for penetration of foundations into soil. Comput Geotech 2008;35(3):372–82.
[55] Zhou H, Randolph MF. Computational techniques and shear band development for cylindrical and spherical penetrometers in strain-softening clay. Int J Geomech 2007;7(4):287–95.
[56] Zhou H, Randolph MF. Resistance of full-flow penetrometers in rate-dependent and strain-softening clay. Geotechnique 2009;59(2):79–86.
[57] Zhou H, Randolph MF. Large deformation analysis of suction caisson installation in clay. Can Geotech J 2006;43(12):1344–57.